http://www.kidney-international.org

see commentary on page 1494

Aquaporin-1 plays an essential role in water permeability and ultrafiltration during peritoneal dialysis

J Ni[1], J-M Verbavatz[2], A Rippe[3], I Boisdé[2], P Moulin[1], B Rippe[3], AS Verkman[4] and O Devuyst[1]

[1]Division of Nephrology and Department of Pathology, UCL Medical School, Brussels, Belgium; [2]DBJC/SBFM, CEA Saclay, Gif-sur-Yvette, France; [3]Department of Nephrology and Physiology, University Hospital of Lund, Sweden and [4]Departments of Medicine and Physiology, UCSF, San Francisco, California, USA

The water channel aquaporin-1 (AQP1) is considered as the molecular counterpart of the ultrasmall pore predicted by the three-pore model of fluid transport across the peritoneal membrane. However, the definitive proof of the implication of AQP1 in solute-free water transport, sodium sieving, and ultrafiltration (UF) during peritoneal dialysis (PD) is lacking, and the effects of its deletion on the structure of the membrane are unknown. Using real-time reverse transcriptase-polymerase chain reaction and immunogold electron microscopy, we showed that AQP1 is the most abundant member of the AQP gene family expressed in the mouse peritoneum, and the only one located in the capillary endothelium. Transport studies during a 2-h dwell demonstrated that, in comparison with *Aqp1*$^{+/+}$ littermates, *Aqp1*$^{-/-}$ mice had no sodium sieving; an ~70% decrease in the initial, solute-free UF; and an ~50% decrease in cumulative UF. These modifications occurred despite unchanged osmotic gradient and transport of small solutes in the *Aqp1*$^{-/-}$ mice. Heterozygous *Aqp1*$^{+/-}$ mice showed intermediate values in sodium sieving and initial UF, whereas cumulative UF was similar to *Aqp1*$^{+/+}$ mice. The deletion of AQP1 had no effect on the expression of other AQPs and on the density, structure, or diameter of peritoneal capillaries. These data provide direct evidence for the role of AQP1 during PD. They validate essential predictions of the three-pore model: (i) the ultrasmall pores account for the sodium sieving, and (ii) they mediate 50% of UF during a hypertonic dwell.

Kidney International (2006) **69,** 1518–1525. doi:10.1038/sj.ki.5000285; published online 1 March 2006

KEYWORDS: water channel; sodium sieving; capillary endothelium; three-pore model

Correspondence: *O Devuyst, Division of Nephrology, UCL Medical School, 10 Avenue Hippocrate, B-1200 Brussels, Belgium.*
E-mail: devuyst@nefr.ucl.ac.be

Received 25 July 2005; revised 30 October 2005; accepted 18 November 2005; published online 1 March 2006

The capacity for ultrafiltration (UF) across the peritoneal membrane is a major predictor of outcome and mortality in peritoneal dialysis (PD) patients.[1,2] Failure of this UF capacity is the most frequent abnormality in long-term PD patients, and the main reason for technical failure.[3] Fifteen years ago, B Rippe and co-workers proposed a 'three-pore' model based on computer simulations to describe the exchange of fluid across the peritoneal membrane.[4,5] This model has become an essential tool for PD, as it provides a comprehensive method for monitoring individual patients over time and adjusting dialysis prescription.[6]

The three-pore model predicts that the major transport barrier of the peritoneum is the capillary endothelium.[4–6] The 'small pores' (radius 40–50 Å), which correspond to the clefts located between endothelial cells, account for ~95% of the hydraulic conductance (UF coefficient, L_pS). A second population of pores, the 'large pores' (radius 250 Å), thought to correspond to the venular interendothelial gaps, accounts for 5% of the UF coefficient. These pores are involved in the transport of macromolecules and, although they represent only 0.01% of the total number of pores, they mediate an important part of the UF via convection of plasma from blood to the peritoneal cavity. The third population of pores consists in water-specific, 'ultrasmall pores' located in the endothelial cells. The ultrasmall pores account only for 1–2% of the hydraulic conductance, meaning an almost insignificant contribution to the overall UF coefficient. However, because they reject solutes but facilitate the transport of water, the ultrasmall pores are extremely important during crystalloid osmosis. Thus, they have been predicted to mediate half of the UF, as well as the 'sodium sieving', that is, the fall in dialysate sodium concentration, during a dwell with hypertonic glucose.[5,6] Understanding the molecular counterpart and the role of the ultrasmall pores has a major clinical importance, since the link between the integrity of the ultrasmall pores and the UF capacity and sodium sieving remains a much debated question in PD.[7–9]

According to the three-pore model, the ultrasmall pore should be located in the endothelium lining peritoneal capillaries and postcapillary venules, where occurs most of

the water movement during PD. It should also facilitate water movement while being unpermeable to glucose and glycerol, hence have a minimal radius <3 Å. The identification of the aquaporins, a family of integral plasma membrane proteins found in bacteria, plants, and mammals, provided critical insights in the molecular mechanisms involved in water permeation across biological membranes.[10] The first identified member of this family was aquaporin-1 (AQP1), whose distribution includes red blood cells, renal tubular epithelial cells, and endothelial cells.[11,12]

AQP1 is distributed in the endothelium lining capillaries, venules and small veins of the peritoneum.[13,14] The pore formed by AQP1,[15] the inhibition of water permeability by $HgCl_2$,[16,17] and the reduced osmotically-induced water transport in mice lacking AQP1 but not in mice lacking AQP4[18] supported the hypothesis that AQP1 is the molecular counterpart of the ultrasmall pore. However, in the absence of a methodology adequate for transport studies in mouse, most of the evidence for the role of AQP1 in the peritoneum thus far was still indirect and/or incomplete. Furthermore, the expression profile of the AQP gene family, the role of AQP1 in UF and sodium sieving, the effect of AQP1 deletion on the transport of small solutes, and the structural modifications and compensatory mechanisms in the peritoneum of AQP1 knockout (KO) mice have not been investigated.

In this study, we have characterized the expression pattern of the AQP gene family in the mouse peritoneum and have used a meticulous infusion model[19,20] to provide a direct evidence of the role of AQP1 in transport across the peritoneal membrane. Our data validate the predictions of the three-pore model and give new insights in the regulation of AQP1 and microvascular permeability.

RESULTS

Clinical and biological parameters of the AQP1 mice

In comparison with wild-type littermates, *Aqp1*$^{-/-}$ mice had lower body weight, plasma urea, and MAP, whereas intermediate values were observed in *Aqp1*$^{+/-}$ mice (Table 1). As previously described,[21] the *Aqp1*$^{-/-}$ mice had an impaired ability to concentrate urine, as evidenced by polyuria. The latter was compensated by increased water intake (*Aqp1*$^{-/-}$: 17.7 ± 1.3 ml/24 h vs *Aqp1*$^{+/+}$: 6.5 ± 0.3 ml/24 h, $P<0.0001$, $N=5$ pairs), explaining why plasma sodium levels were similar in both groups (Table 1). The mice had similar hematocrit, plasma albumin, and NO_x levels in the dialysate (*Aqp1*$^{+/+}$: 43 ± 3 mM vs *Aqp1*$^{-/-}$: 46 ± 4 mM).

Expression patterns of the AQP gene family in the mouse peritoneum

Real-time RT–PCR analyses (Figure 1) showed that AQP1 was the most abundant isoform in the visceral peritoneum of *Aqp1*$^{+/+}$ mice. A significant expression of AQP7 was also detected, as well as very low levels of AQP9 and AQP5, and traces of AQP3 (more than 500-fold less than AQP1). The deletion of AQP1 was not reflected by significant changes in the expression of the other AQPs in the peritoneum (Figure 1).

Expression of AQP1 and endothelial markers

The core and glycosylated AQP1 isoforms were identified by immunoblotting in the visceral peritoneum of *Aqp1*$^{+/+}$ mice (Figure 2). Of note, AQP1 was apparently less glycosylated in the peritoneum than in kidney samples, possibly reflecting the exclusive endothelial expression in the former tissue. Densitometry analysis confirmed an $\sim$50% reduction in the expression of AQP1 in the peritoneum of *Aqp1*$^{+/-}$ mice (in arbitrary units: 3236 ± 276 vs 6405 ± 192, respectively, $N=4$ pairs). The deletion of AQP1 in the peritoneum was not reflected by significant modifications in

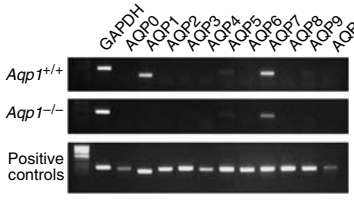

mRNA	Threshold (C_t)	
	Aqp1$^{+/+}$	*Aqp1*$^{-/-}$
GAPDH	17.2±0.1	17.2±0.2
AQP0	ND	ND
AQP1	21.8±0.2	ND
AQP2	ND	ND
AQP3	30.8±0.8	ND
AQP4	ND	ND
AQP5	27.9±0.4	26.2±0.4
AQP6	ND	ND
AQP7	22.9±0.2	23.4±0.2
AQP8	ND	ND
AQP9	27.8±0.3	29.6±0.4
AQP10	ND	30.9±0.3

Figure 1 | Expression patterns of the AQP gene family in the mouse peritoneum: semiquantitative and real-time RT-PCR. Left panel: Representative semiquantitative RT-PCR analysis of the expression of the AQP gene family in the visceral peritoneum of *Aqp1*$^{+/+}$ and *Aqp1*$^{-/-}$ mice. Equal amounts (20 μl) of PCR products were loaded in each lane of a 1.5% agarose gel. Positive control tissues were from the lens (AQP0); kidney (AQP1, AQP2, AQP3, AQP4, AQP6); lung (AQP5); adipose tissue (AQP7); liver (AQP8, AQP9); and small intestine (AQP10). The size of amplicons is given in Table 3. Right panel: Real-time RT-PCR quantification for mRNA expression of the AQP gene family members in the mouse peritoneum. The threshold Ct values (number of cycles needed to generate a signal above the predefined threshold) were obtained from five different mice in each group. ND, transcript not detected or Ct > 31 cycles. The quantitative difference between two transcripts equals [$2^{\Delta Ct}$].

Table 1 | Baseline clinical and biological parameters in the AQP1 mice

Groups	*N*	Body weight (g)	Plasma sodium (mM)	Plasma urea (mg/dl)	MAP (mm Hg)
Aqp1$^{-/-}$	6	26.1 ± 1.0[a]	152 ± 1	15 ± 1[a]	80 ± 2[a]
Aqp1$^{+/+}$	6	30.1 ± 0.8	151 ± 2	21 ± 1	95 ± 3
Aqp1$^{+/-}$	6	28.9 ± 0.9	153 ± 1	18 ± 1	88 ± 4

MAP, mean arterial blood pressure; all parameters were obtained before the dwell (T0).
[a]$P<0.05$ vs *Aqp1*$^{+/+}$.

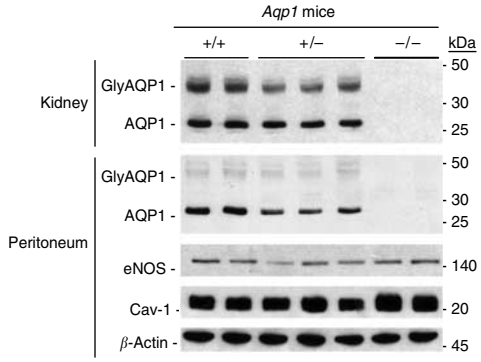

Figure 2 | Expression of AQP1 and endothelial markers: immunoblotting. Representative immunoblots for AQP1 (1:20 000) in kidney and peritoneum extracts prepared from *Aqp1*$^{+/+}$, *Aqp1*$^{+/-}$ and *Aqp1*$^{-/-}$ mice (20 μg protein/lane). The blots were stripped and reprobed with a monoclonal antibody against β-actin (1:10 000) for loading accuracy. The core (28 kDa) and glycosylated (35–50 kDa) AQP1 isoforms are identified in the kidney and peritoneum of Aqp1$^{+/+}$ mice, whereas an intermediate signal is observed in heterozygotes and no signal is detected in the Aqp1$^{-/-}$ mice. Note the *lower* abundance of glycosylated AQP1 isoforms in peritoneum vs kidney samples. The expression of eNOS (1:5000) and caveolin-1 (1:2500) was also tested in the same peritoneal samples and showed no significant difference.

the endothelial proteins, endothelial nitric oxide synthase (eNOS), and caveolin-1, as confirmed by densitometry analysis (data not shown).

Influence of AQP1 deletion on the structure of the peritoneal membrane

Morphological examination showed that the deletion of AQP1 was not reflected by structural changes in the visceral and parietal peritoneum at baseline (Figure 3a). Morphometry analysis demonstrated that the thickness of the submesothelial area was similar in both groups (average thickness: 14.4 ± 0.7 μm in *Aqp1*$^{+/+}$ mice vs 15.3 ± 1.4 μm in *Aqp1*$^{-/-}$ mice; $N = 7$ pairs; see Figure 3a, insets), supporting the conclusion that the mesothelium and associated connective tissue do not affect the osmotic filtration and small solutes transport.[9]

Immunostaining (Figure 3b) showed that AQP1 is exclusively located in the endothelium lining peritoneal capillaries and venules of *Aqp1*$^{+/+}$ mice, whereas no specific staining was detected in the mesothelium. Morphometry analysis on four pairs of CD31-stained sections confirmed that the vascular density was not significantly modified by the deletion of AQP1. No specific staining was detected for AQP3, AQP5, AQP7, and AQP9 (data not shown).

Immunogold electron microscopy and ultrastructural examination

Using immunogold EM (Figure 4), we detected a strong labeling for AQP1 in the endothelial cells lining peritoneal capillaries (Figure 4a). The labeling for AQP1 was detected along the plasma membrane and numerous infoldings in endothelial cells. No staining was detected in the mesothelial cells. The AQP1 labeling was significantly weaker in heterozygous mice (Figure 4b) and, as expected, abolished in the *Aqp1*$^{-/-}$ mice (Figure 4c). The AQP1 labeling was far stronger in the plasma membranes of endothelial cells than in red blood cells (Figure 4f), as confirmed by morphometry (density of AQP1 gold particles in the capillary endothelium, per μm cell length: 20 ± 3.4 in *Aqp1*$^{+/+}$ mice ($N = 14$) vs 9.8 ± 1.8 in *Aqp1*$^{+/-}$ mice ($N = 9$) vs 2.2 ± 0.2 in the red blood cell of *Aqp1*$^{+/+}$ mice ($N = 10$); $P < 0.05$ for all comparisons). No labeling for AQP3 (nor AQP7 and AQP9) was detected in red blood cells, endothelial cells, and mesothelial cells, either in *Aqp1*$^{+/+}$ (Figure 4g and h) or *Aqp1*$^{-/-}$ mice (Figure 4i and j).

The ultrastructure of capillary endothelial cells (Karnovski staining) was similar in *Aqp1*$^{+/+}$ (Figure 4d) and *Aqp1*$^{-/-}$ (Figure 4e) mice. The endothelial cells exhibited numerous caveolae and plasma membrane infoldings, and neither the thickness of the cells nor the diameter of capillaries was significantly modified (internal capillary diameter in μm: 2.9 ± 0.2 in *Aqp1*$^{+/+}$ mice ($N = 11$) vs 2.9 ± 0.4 in *Aqp1*$^{-/-}$ mice ($N = 9$)).

Role of AQP1 in UF and small solute transport during PD

We used a PET adapted for the mouse[19,20] to investigate the effects of AQP1 deletion on transport across the peritoneum (Table 2; Figure 5). In *Aqp1*$^{+/+}$ mice, exposure to the dialysate induced a typical sodium sieving (Figure 5a), a progressive reabsorption of glucose from the dialysate (Figure 5b), and a net UF (Table 2). The *Aqp1*$^{-/-}$ mice showed a complete loss of sodium sieving and an $\sim$50% decrease in net UF, whereas glucose reabsorption from dialysate and D/P osmolality at 30 min were unchanged. In comparison with wild-type mice, *Aqp1*$^{+/-}$ mice showed an $\sim$25% decrease in sodium sieving ($P = 0.06$), whereas the net UF values obtained at the end of the 2-h dwell were similar. Of note, small solute transport parameters (evaluated by mass transfer area coefficient of urea and D_{120}/D_0 glucose) were similar in the three groups of AQP1 mice. The qualitative differences in peritoneal transport parameters were verified in different groups of mice, irrespective of gender, inflow volume (2.0 vs 2.5 ml) and glucose concentration (7% vs 3.86%) in the dialysate (data not shown).

The intraperitoneal volume curves were assessed using a ^{125}I-human serum albumin dilution technique.[22] The total ^{125}I-human serum albumin masses retrieved from the peritoneal cavity after 30 s were similar in all genotypes (96 ± 2% in *Aqp1*$^{+/+}$, 97 ± 3% in *Aqp1*$^{-/-}$, and 96 ± 1 % in *Aqp1*$^{+/-}$, $N = 3$ in each group), as were the total protein loss in the dialysate at the end of the dwell (3.8 ± 0.3 mg in *Aqp1*$^{+/+}$, 3.8 ± 0.2 mg in *Aqp1*$^{-/-}$, and 4.3 ± 0.3 mg in *Aqp1*$^{+/-}$, $N = 6$ in each group). The average curves (Figure 5c) obtained in the *Aqp1*$^{-/-}$ mice were significantly lower than in the *Aqp1*$^{+/+}$ and *Aqp1*$^{+/-}$ mice. The initial UF rates were clearly distinct: 33.5 ± 1.8 μl/min for *Aqp1*$^{+/+}$, 22.2 ± 1.3 μl/min for *Aqp1*$^{+/-}$, and 10.1 ± 0.6 μl/min for *Aqp1*$^{-/-}$ mice (Figure 5d). The volume curves were closely

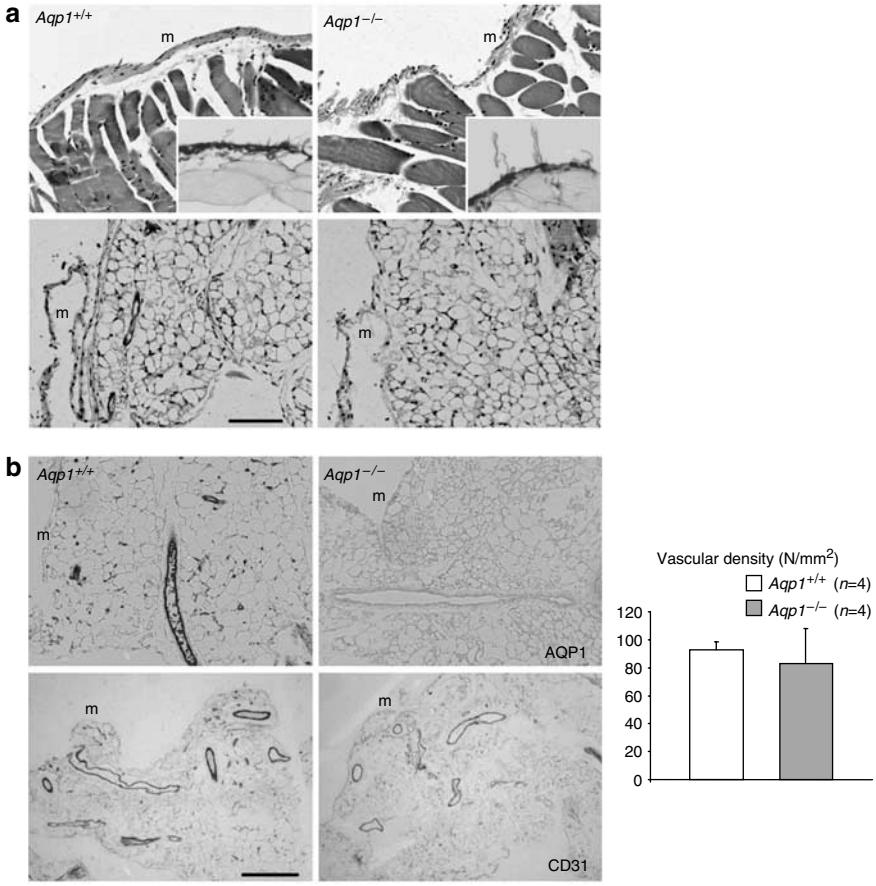

Figure 3 | Structure and vascular density of the peritoneal membrane. (**a**) Hemalun–eosine staining in the parietal (upper panels) and visceral peritoneum (lower panels) of *Aqp1*$^{+/+}$ and *Aqp1*$^{-/-}$ mice shows that the deletion of AQP1 is not reflected by structural changes of the peritoneal membrane. Insets: representative sections of the submesothelial area in the parietal peritoneum (Sirius red staining) at higher magnification, showing a similar thickness in both groups. (**b**) The immunoreactivity for AQP1 (1:200; upper panels) is located in the endothelium lining peritoneal capillaries and venules in *Aqp1*$^{+/+}$ mice, whereas no staining is detected in the mesothelium. As expected, there was no labeling in *Aqp1*$^{-/-}$ mice. The density of capillaries and blood vessels stained for the endothelial marker CD31 (1:50; lower panels) is similar in *Aqp1*$^{+/+}$ and *Aqp1*$^{-/-}$ mice. The morphometry analysis in the visceral peritoneum (CD31 staining) confirmed that the vascular density (in vessels/mm^2: 93 ± 6 in *Aqp1*$^{+/+}$ mice vs 83 ± 25 in *Aqp1*$^{-/-}$ mice) (right panel) is not modified by the deletion of AQP1. Bar = 100 μm; m, mesothelium; the genotype is indicated in the upper left corner.

similar, at least during 0–60 min, to those computer simulated by the three-pore model of peritoneal transport by rescaling all relevant exchange parameters by $BW^{0.7}$ (using a scaling factor of 230 from man to mouse) (data not shown). The initial UF rate significantly correlated with the sodium sieving obtained in the same mice (regression: $y = 2.563 + 0.21x$, $r = 0.71$, $P = 0.001$).

DISCUSSION

A prerequisite of the three-pore model is the existence of ultrasmall pores in the endothelium lining peritoneal capillaries.[5] These pores are predicted to be responsible for the sodium sieving and up to 50% of the UF during a hypertonic dwell.[5,6] Our data provide a direct demonstration that AQP1 mediates the initial, solute-free water transport (assessed clinically by the sodium sieving) as well as half of the UF during PD in mouse. The modifications observed in *Aqp1*$^{-/-}$ mice occur without changes in the osmotic gradient, and without affecting the microvascular structure and density in the peritoneal membrane.

Previous studies in *Aqp1*$^{-/-}$ mice have shown that AQP1 plays a role in osmotically driven water permeability in microvessels lining distal airways[23] and in the descending vasa recta.[24] In contrast, the deletion of AQP1 in the endothelium of salivary glands has no effect on salivary fluid production.[25] A preliminary study showed that AQP1 is involved in the osmotically induced water transport across the peritoneal membrane.[18] However, that study did not address the contribution of AQP1 in the sodium sieving and UF, the possibility of compensatory mechanisms, and the situation in heterozygous mice. The present study addressed these questions, using a well-characterized infusion model on the AQP1 mouse.[19,20]

The functional loss of AQP1 is traditionally considered as a potential cause of a loss of sodium sieving.[26] This hypothesis, however, has been challenged by the apparently

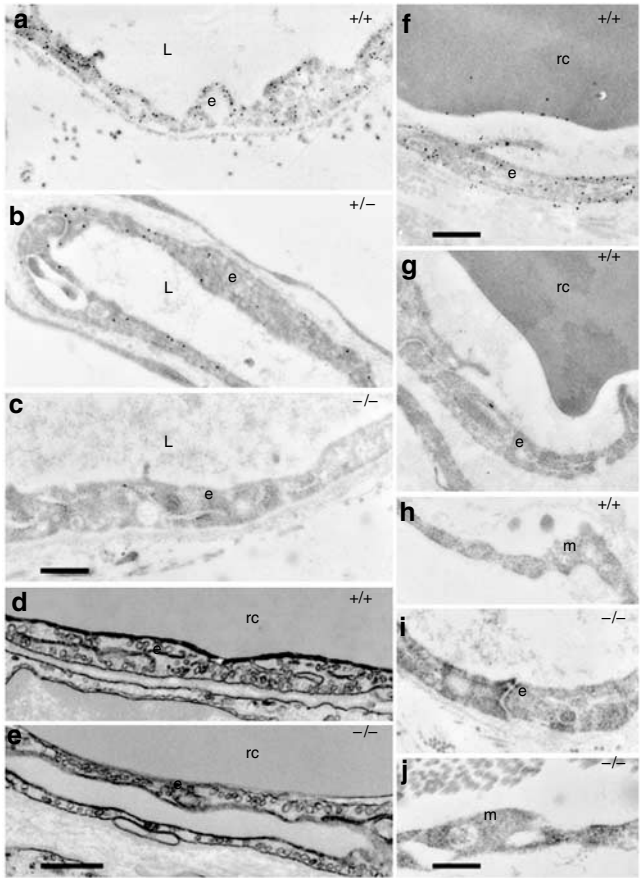

Figure 4 | Immunogold electron microscopy and ultrastructural examination of the endothelium in the peritoneum of *Aqp1*$^{+/+}$ and *Aqp1*$^{-/-}$ mice. (**a–c**) Immunogold labeling on mouse visceral peritoneum revealed a very strong signal for AQP1 in plasma membranes and plasma membrane infoldings of capillary endothelial cells in (**a**) *Aqp1*$^{+/+}$ mice. (**b**) The AQP1 labeling was markedly weaker in heterozygous mice, but remained easily detectable. No labeling was detected in (**c**) *Aqp1*$^{-/-}$ mice, demonstrating the specificity of labeling with this antibody. (**f**) Comparison of the labeling density in wild-type mice shows that AQP1 labeling is markedly stronger in endothelial cells than in red blood cells. No AQP1 labeling was detected in mesothelial cells. (**d, e**) Karnovski staining of epon sections of mouse parietal peritoneum shows that capillary endothelial cells exhibit numerous caveolae and plasma membrane infoldings both in (**d**) *Aqp1*$^{+/+}$ and (**e**) *Aqp1*$^{-/-}$ mice. No difference in the ultrastructure of capillaries or veinules was detected between genotypes. (**g–j**) No labeling for AQP3 was detected in red blood cells, endothelial cells and mesothelial cells, either in (**g, h**) *Aqp1*$^{+/+}$ or (**i, j**) *Aqp1*$^{-/-}$ mice. Bars = 500 nm; e, endothelium; m, mesothelium; rc, red blood cell; l, capillary lumen. The AQP1 genotype is indicated in the upper right corner.

intact expression of AQP1 in such patients.[27,28] Similarly, the link between UF failure and integrity of AQP1 remains debated.[6,8,9,28] The present study provides a direct answer, by showing that the deletion of AQP1 induces a loss of sodium sieving, with a close relationship between the level of AQP1 expression and the initial, solute-free UF rate (Figure 5). Also, these results provide a mirror image of previous data showing that pharmacological induction of AQP1 expression is reflected by an increased sodium sieving.[29] The residual initial UF rate in the *Aqp1*$^{-/-}$ mice suggests that a non-AQP1 pathway participates in the initial osmotic water flux across the endothelium – similar to what has been postulated in the descending vasa recta.[24] The identity of this alternative water pathway remains to be defined. The lack of variation of the submesothelial area thickness confirms that the mesothelium

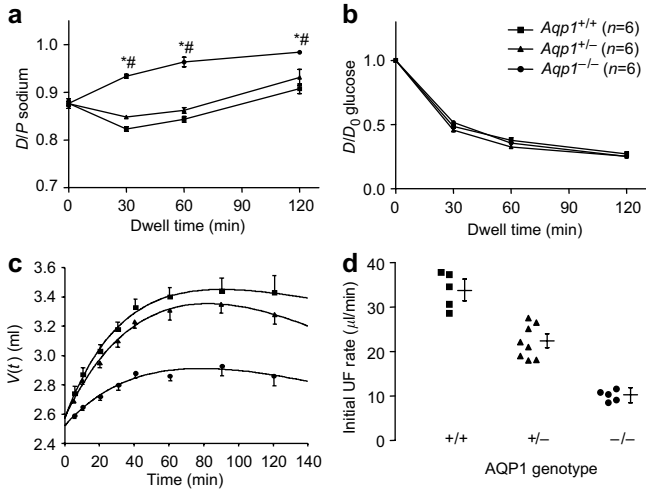

Figure 5 | Effect of AQP1 deletion on water and solute transport parameters. (**a**) The dialysate-to-plasma (D/P) ratio of sodium, (**b**) the progressive removal of glucose from the dialysate (D/D_0 glucose, (**c**) the volume vs time [$V(t)$] curves, and (**d**) the initial UF rates calculated from the first derivate of the best fitting curves for each mouse were determined in *Aqp1*$^{+/+}$ mice (black squares), *Aqp1*$^{+/-}$ mice (black triangles), and *Aqp1*$^{-/-}$ mice (black circles) during a 2-h exchange with 2 ml of 7% glucose dialysate. In comparison with *Aqp1*$^{+/+}$ mice, mice lacking AQP1 show a complete loss of sodium sieving, whereas the glucose reabsorption from dialysate is unchanged. *Aqp1*$^{-/-}$ mice also show significantly lower volume curves and initial UF rates. Intermediate values of sodium sieving and initial UF rates are observed in *Aqp1*$^{+/-}$ mice. $^{*}P < 0.05$ vs *Aqp1*$^{+/+}$ mice and $^{\#}P < 0.05$ vs *Aqp1*$^{+/-}$ mice.

Table 2 | Water and small solute transport in the AQP1 mice

Groups	*N*	Net UF/BW (μl/g)	P_{30} sodium (mM)	D_{30} sodium (mM)	Sodium sieving (%)	D_{30}/P_{30} osmolality	MTAC urea[a] (μl/min)
Aqp1$^{-/-}$	6	27 ± 1.8[b,c]	146 ± 1	137 ± 1[b,c]	−6.5 ± 1.0[b,c]	1.34 ± 0.09	33 ± 1.0
Aqp1$^{+/+}$	6	58 ± 3.1	147 ± 2	123 ± 2	6.0 ± 1.3	1.28 ± 0.03	28 ± 2.5
Aqp1$^{+/-}$	6	57 ± 2.0	148 ± 1	126 ± 1	3.1 ± 0.9	1.26 ± 0.02	29 ± 4.0

BW, body weight; D_{30}, dialysate concentration at 30 min; P_{30}, plasma concentration at 30 min; sodium sieving=$(D_0/P_0–D_{30}/P_{30})/D_0/P_0 \times 100$ (in %); UF, ultrafiltration;
[a]MTAC, mass transfer area coefficient ((μl/min) of urea, according to the Garred two-sample model.[20]
[b]$P < 0.05$ vs *Aqp1*$^{+/+}$.
[c]$P < 0.05$ vs *Aqp1*$^{+/-}$.

and associated connective tissue do not affect the osmotic filtration.[9]

Our data validate a second prediction of the three-pore model, that is, that AQP1 mediates ~50% of the net UF during a hypertonic dwell,[5,6] without affecting the small solute transport rate. Although apparently surprising, the fact that the cumulative UF is not decreased in the heterozygous *Aqp1*$^{+/-}$ mice was also predicted by the three-pore model. Indeed, changes in the initial water transport must be dissociated from the cumulative UF after a long dwell (a 2 h-dwell in mouse corresponds to a 6–8 h-dwell in man).[5,6] The cumulative UF depends from different variables, including availability of the small pores and a sustained osmotic gradient. Accordingly, a reduction in the UF coefficient accounted for by aquaporins (i.e. the situation of the *Aqp1*$^{+/-}$ mice) will not affect the cumulative UF after a long dwell: the simulated volume curves corresponding to control or reduced aquaporins eventually converge over time, resulting in similar UF.[30] These data may have an important clinical implication, since they suggest that the water transport mediated by AQP1 is particularly important in short dwells, for instance those performed in automated PD.

AQP1 is the most abundant AQP transcript in the mouse peritoneum, and the sole isoform detected in the endothelium lining peritoneal capillaries and post-capillary venules, the principal location for fluid exchange in PD.[31] Immunogold EM studies revealed that AQP1 expression is ~10-fold stronger in the plasma membrane of endothelial cells than red blood cells. On the basis of such expression levels, one could expect that the deletion of AQP1 may lead to adaptative changes in the microvasculature. For instance, the descending vasa recta in the medulla of *Aqp1*$^{-/-}$ mice are remarkably larger in diameter, which could participate in increasing the medullary blood flow.[24] Yet, the deletion of AQP1 is not reflected by changes in the density, structure, or diameter of peritoneal capillaries. This observation is actually not surprising when considering that the permeability of the peritoneum is only challenged during PD, that is, when an osmotic agent is instilled in the peritoneal cavity. In contrast, the vasa recta are constantly exposed to large osmotic gradients in the kidney medulla. In agreement with our previous studies,[19] the lack of modification of the small solute transport in the *Aqp1*$^{-/-}$ mice probably reflects the lack of modification in microvascular density and the stability of eNOS expression and NO_x levels in these mice.

As described in the original colony,[21] mice lacking AQP1 show a 15% drop in blood pressure (MAP). Studies in PD patients showed that a ~20% lowering of blood pressure with ACE inhibitors has no significant effect in drain volume and glucose absorption during PD.[32] Studies in rat models showed that even large (up to 60%) blood flow reduction has no significant effect on the osmotic water flow across the peritoneum.[33] In control mice,[20] as well as in the *Aqp1*$^{+/+}$ mice used here, an experimental decrease in MAP had no effect on UF. The lack of effect of blood pressure changes on transport parameters is probably explained by the fact that the endothelium is in series with the interstitium, which blunts the effect of blood pressure lowering on UF.[9]

The putative role of aquaporins other than AQP1 in the peritoneum has also been debated. The real-time RT-PCR analysis confirms that AQP1 is the most abundant transcript in mouse peritoneum, whereas the non-endothelial AQP7 (adipose tissue), AQP9 (leukocytes), and AQP3/AQP5 (macrophages, dendritic cells) were detected with much lower intensity. Using immunogold EM, we showed that AQP1 is exclusively located in the endothelium and is not detected in mesothelial cells. These results, which confirm previous studies in mouse[19,20] and rat,[29] contrast with the inconsistent staining for AQP1 observed in rat and human mesothelium.[14,34,35] The discrepancy could be explained by the state of cell differentiation, or the osmo-induction of AQP1 in mesothelial cells.[35,36] Because the mesothelium does not represent a significant functional barrier for water transport in PD, the importance of AQP1 at that level is unclear. A similar conclusion can be drawn regarding the putative role of aquaglyceroporins (AQP3/AQP7/AQP9) in the peritoneum. The nonendothelial distribution of these isoforms and the fact that glycerol is an effective osmotic agent argue against their functional role in transport during PD.

In conclusion, the data presented here validate essential predictions of the three-pore theory and provide a direct demonstration of the critical role played by AQP1 in the sodium sieving and UF during PD. They also give novel insights in the molecular mechanisms operating in the peritoneal membrane and the capillary endothelium in general.

MATERIALS AND METHODS

Animals

Mice lacking AQP1 were generated as previously described.[21] We used gender-matched littermates, aged 8–12 weeks. All animals had access to standard diet and tap water *ad libitum*. The experiments were conducted in accordance with the National Research Council Guide for the Care and Use of Laboratory Animals and the local Ethics Committee.

Peritoneal transport studies and tissue sampling

Transport across the mouse peritoneum was investigated using a modified PET with 7% glucose-based dialysate (2.0 ml; Dianeal^{R}, Baxter, Nivelles, Belgium) as described previously.[19,20] Blood and dialysate samples were taken at time 0, 30, 60, and 120 min of the dwell. Net UF was measured at the end of the dwell. The transport of small solutes was evaluated by the mass transfer area coefficient of urea, according to the Garred two-sample model,[20] and the D_{120}/D_0 glucose. Other parameters were assayed as described.[20] The level of nitrite and nitrate (NO_x) was measured using the Griess reaction (Cayman Chemical, Ann Arbor, MI, USA).

To obtain volume curves and initial UF rates, the peritoneal cavity was infused with 2.5 ml of 3.86% glucose dialysate containing 50 μl of 10% bovine serum albumin and 50 μl of ^{125}I-human serum albumin. Dialysate and blood samples (10 μl) were counted in a

γ-counter (Canberra, Meriden, CT, USA). Intraperitoneal volume as a function of dwell time [$V(t)$] was assessed as described previously.[22] Preliminary experiments verified that the rapid peritoneal adsorption of ^{125}I-human serum albumin was similar in all groups of mice. The initial UF rates were calculated according to Stelin and Rippe.[4] The best fitting volume curve was calculated using nonlinear least-squares regression analysis. At the end of the dwell, mice were killed by exsanguination and samples were processed for fixation (parietal and visceral peritoneum) and mRNA/protein extraction (visceral peritoneum).

RT-PCR and semiquantitative real-time RT-PCR

Total RNA from mouse visceral peritoneum was extracted with Trizol (Invitrogen, Merelbeke, Belgium), treated with DNase I and reverse-transcribed into cDNA. The primers are given in Table 3. Changes in target genes mRNA levels were determined by semiquantitative real-time RT-PCR with an iCycler IQ System (Bio-Rad Laboratories, Hercules, CA, USA) using SYBR Green I detection as described.[20] All reactions were performed in duplicate. The PCR conditions were 94°C for 3 min followed by 31 cycles of 30 s at 95°C, 30 s at 61°C and 1 min at 72°C. To exclude amplification from contaminating genomic DNA, samples of RNA that had not been reverse-transcribed were run in parallel PCR reaction. Standards curves were prepared by serial four-fold dilutions of cDNA samples for each assay. The efficiency of the reactions was calculated from the slope of the standard curve [efficiency $= (10^{-1/\text{slope}}) - 1$].

Antibodies

We used a rabbit antibody against AQP1 (Chemicon International, Temecula, CA, USA); a monoclonal antibody against eNOS (Transduction laboratories, Lexington, KY, USA); a goat antibody against CD31 (Santa Cruz Biotechnology, Santa Cruz, CA, USA); polyclonal antibodies against AQP3,[37] AQP5,[38] AQP7 and AQP9 (Chemicon, Temecula, CA, USA); a rabbit antibody against caveolin-1 (BD Biosciences, Erembodegem, Belgium); and a monoclonal antibody against β-actin (Sigma, St Louis, MO, USA).

Table 3 | Sequences of primers and efficiency of RT-PCR reactions

Gene	Sequence of primers	Amplicons (bp)	Efficiency[a]
GAPDH	Sense TGCACCACCAACTGCTTAGC	176	1.04 ± 0.03
	Antisense GGATGCAGGGATGATGTTCT		
AQP0	Sense TTCTGGCCTTTACCCTGCTT	150	0.99 ± 0.04
	Antisense TCCCACCAGACCTCCTAAC		
AQP1	Sense GCTGTCATGTACATCATCGCCCAG	107	1.03 ± 0.04
	Antisense AGGTCATTGCGGCCAAGTGAAT		
AQP2	Sense TCACTGGGTCTTCTGGATCG	147	1.03 ± 0.04
	Antisense CGTTCCTCCCAGTCAGTGT		
AQP3	Sense GGGCTTCAATTCTGGCTATG	153	1.00 ± 0.01
	Antisense GAAGACACCAGCGATGGAAC		
AQP4	Sense TGTGCACACGAAAGATCAGC	144	1.03 ± 0.02
	Antisense TTCCATGAACCGTGGTGACT		
AQP5	Sense TGGAGCAGGCATCCTGTACT	151	0.98 ± 0.01
	Antisense CGTGGAGGAGAAGATGCAGA		
AQP6	Sense GGTCCACAACAGCACATCAA	143	1.02 ± 0.06
	Antisense GTGCCACAGAGGTTCCAATC		
AQP7	Sense CCTGAGTGCTGGGGATACA	146	1.04 ± 0.02
	Antisense AGACATTCCCCCTTGACACC		
AQP8	Sense ATGGCTGGCTACTGGGACTT	145	1.01 ± 0.01
	Antisense CGCCAGCAGTTCTTCTTCAC		
AQP9	Sense TATCCCCAGAAGCCCAAACT	145	0.93 ± 0.01
	Antisense GCTGTTGGGATCAAACTGGA		
AQP10	Sense GGGGTTGCTTCCTAAGTGCT	151	0.93 ± 0.01
	Antisense GACAAAGGGAGGGGTCAGA		

[a]The efficiency of the reactions was calculated from the slope of the standard curve [efficiency=$(10^{-1/\text{slope}})$–1].

Immunoblotting

SDS-PAGE and immunoblotting were performed as described.[19,20] The membranes were blocked for 30 min, incubated overnight with the primary antibody at 4°C, washed, incubated for 1 h with secondary antibodies (Dako, Glostrup, Denmark), and visualized with enhanced chemiluminescence (Amersham, Little Chalfont, UK). Densitometry analysis was performed using the NIH-Image V1-57 software.[20,21]

Tissue staining and immunohistochemistry; quantification of vascular density

Samples from the visceral and parietal peritoneum were fixed in 4% paraformaldehyde and embedded in paraffin. Staining (hemalun–eosine and Sirius red) and immunostaining were performed as previously described.[19,34] Sections were viewed under a Leica DMR coupled to a Leida DC 300 camera (Leica, Heerbrugg, Switzerland). Microvascular density was assessed using CD31 immunostaining.[39] Sections were digitalized to measure the vascular density (in N vessels/mm^2),[19] in four pairs of mice (mean of 10 fields per sample). A similar method was used to measure the thickness of the submesothelial area of the parietal peritoneum (Sirius red staining) in seven pairs of mice.

Transmission electron microscopy

Mouse peritoneum was processed for ultrastructural studies and immunogold labelling as previously reported.[20,29] Samples were fixed in 4% parafomaldehyde and embedded either in Unicryl (gold labeling) or in epon (Karnovski staining). For Karnovski staining, sections were counterstained in 0.2% lead citrate for 1 min. For gold labeling, the sections were incubated with the primary antibody (3 μg/ml final dilution) and, after washing, with a 1:20 dilution of 10 nm of gold-conjugated anti-rabbit antibodies (Amersham), before washing and staining in 5% uranyl acetate followed by lead citrate. The sections were observed on a Philips EM 400 microscope (Fei, Netherlands).

Data analysis

Data are mean ± s.e.m. Comparisons were performed using one-way ANOVA, followed by Bonferroni's multiple comparison test. Significance level was $P < 0.05$.

ACKNOWLEDGMENTS

These studies were supported in part by the Fonds National de la Recherche Scientifique, the Fonds de la Recherche Scientifique Médicale, an Action de Recherche Concertée (ARC 00/05-260), the National Institutes of Health grant DK35124, and grants from Baxter. We thank E Goffin, F Jouret, R Krediet, and B Lindholm for providing invaluable suggestions and critiques; and C Delporte and BJ Baum for providing the anti-AQP5 antibodies. The expert technical assistance of V Beaujean, M Boury-Jamot, Y Cnops, H Debaix, and L Wenderickx is highly appreciated.

Part of these data have been presented during the 2004 annual meeting of the American Society of Nephrology (St Louis, MO, USA, 29 October–1 November 2004), and published in abstract form (*J Am Soc Nephrol* 2004; 15: 16–17A).

REFERENCES

1. Churchill DN, Thorpe KE, Nolph KD *et al.* Increased peritoneal membrane transport is associated with decreased patient and technique survival for continuous ambulatory peritoneal dialysis patients. *J Am Soc Nephrol* 1998; **9**: 1285–1292.
2. Brown EA, Davies SJ, Rutherford P *et al.* Survival of functionally anuric patients on automated peritoneal dialysis: the European APD Outcome Study. *J Am Soc Nephrol* 2003; **14**: 2948–2957.
3. Davies SJ, Phillips L, Griffiths AM *et al.* What really happens to people on long-term peritoneal dialysis? *Kidney Int* 1998; **54**: 2207–2217.
4. Stelin G, Rippe B. A phenomenological interpretation of the variation in dialysate volume with dwell time in CAPD. *Kidney Int* 1990; **38**: 465–472.
5. Rippe B, Stelin G, Haraldsson B. Computer simulations of peritoneal fluid transport in CAPD. *Kidney Int* 1991; **40**: 315–325.
6. Rippe B, Venturoli D, Simonsen O, de Arteaga J. Fluid and electrolyte transport across the peritoneal membrane during CAPD. *Perit Dial Int* 2004; **24**: 10–27.
7. Davies SJ. Monitoring of long-term peritoneal membrane function. *Perit Dial Int* 2001; **21**: 225–230.
8. Smit W, Struijk DG, Ho-Dac-Pannekeet MM, Krediet RT. Quantification of free water transport in peritoneal dialysis. *Kidney Int* 2004; **66**: 849–854.
9. Flessner MF. The transport barrier in intraperitoneal therapy. *Am J Physiol Renal Physiol* 2005; **288**: F433–F442.
10. Agre P. Aquaporin water channels (Nobel Lecture). *Angew Chem Int Edn* 2004; **43**: 4278–4290.
11. Preston GM, Carroll TP, Guggino WB, Agre P. Appearance of water channels in *Xenopus* oocytes expressing red cell CHIP28 protein. *Science* 1992; **256**: 385–387.
12. Nielsen S, Smith BL, Christensen EI, Agre P. Distribution of the aquaporin CHIP in secretory and resorptive epithelia and capillary endothelia. *Proc Natl Acad Sci USA* 1993; **90**(Suppl 1): 7275–7279.
13. Pannekeet MM, Mulder JB, Weening JJ *et al.* Demonstration of aquaporin-CHIP in peritoneal tissue of uremic and CAPD patients. *Perit Dial Int* 1996; **16**: S54–S57.
14. Devuyst O, Nielsen S, Cosyns JP *et al.* Aquaporin-1 and endothelial nitric oxide synthase expression in capillary endothelia of human peritoneum. *Am J Physiol* 1998; **275**: H234–H242.
15. Murata K, Mitsuoka K, Hirai T *et al.* Structural determinants of water permeation through aquaporin-1. *Nature* 2000; **407**: 599–605.
16. Carlsson O, Nielsen S, Zakaria el-R Rippe B. *In vivo* inhibition of transcellular water channels (aquaporin-1) during acute peritoneal dialysis in rats. *Am J Physiol* 1996; **271**: H2254–H2262.
17. Zweers MM, Douma CE, deWaart DR *et al.* Amphotericin B, mercury chloride and peritoneal transport in rabbits. *Clin Nephrol* 2001; **56**: 60–68.
18. Yang B, Folkesson HG, Yang J *et al.* Reduced osmotic water permeability of the peritoneal barrier in aquaporin-1 knockout mice. *Am J Physiol* 1999; **276**: C76–C81.
19. Ni J, Moulin P, Gianello P *et al.* Mice that lack endothelial nitric oxide synthase are protected against functional and structural modifications induced by acute peritonitis. *J Am Soc Nephrol* 2003; **14**: 3205–3216.
20. Ni J, Cnops Y, Debaix H *et al.* Functional and molecular characterization of a peritoneal dialysis model in the C57BL/6J mouse. *Kidney Int* 2005; **67**: 2021–2031.
21. Ma T, Yang B, Gillespie A *et al.* Severely impaired urinary concentrating ability in transgenic mice lacking aquaporin-1 water channels. *J Biol Chem* 1998; **273**: 4296–4299.
22. Zakaria ER, Rippe B. Intraperitoneal fluid volume changes during peritoneal dialysis in the rat. Indicator dilution vs volumetric measurements. *Blood Purif* 1995; **13**: 255–270.
23. Bai C, Fukuda N, Song Y *et al.* Lung fluid transport in aquaporin-1 and aquaporin-4 knockout mice. *J Clin Invest* 1999; **103**: 555–561.
24. Pallone TL, Edwards A, Ma T *et al.* Requirement of aquaporin-1 for NaCl-driven water transport across descending vasa recta. *J Clin Invest* 2000; **105**: 215–222.
25. Ma T, Song Y, Gillespie A *et al.* Defective secretion of saliva in transgenic mice lacking aquaporin-5 water channels. *J Biol Chem* 1999; **274**: 20071–20074.
26. Krediet RT. The physiology of peritoneal solute transport and ultrafiltration. In: Gokal R, Khanna R, Krediet RT, Nolph KD (eds). *Textbook of Peritoneal Dialysis*. Kluwer Academic Publishers: Dordrecht, 2000, pp. 135–172.
27. Goffin E, Combet S, Jamar F *et al.* Expression of aquaporin-1 in a long-term peritoneal dialysis patient with impaired transcellular water transport. *Am J Kidney Dis* 1999; **33**: 383–388.
28. Rippe B, de Arteaga J, Venturoli D. Aquaporins are unlikely to be affected in marked ultrafiltration failure: results from a computer simulation. *Perit Dial Int* 2001; **21**: S30–S34.
29. Stoenoiu MS, Ni J, Verkaeren C *et al.* Corticosteroids induce expression of aquaporin-1 and increase transcellular water transport in rat peritoneum. *J Am Soc Nephrol* 2003; **14**: 555–565.
30. Rippe B, Carlsson O. Role of transcellular water channels in peritoneal dialysis. *Perit Dial Int* 1999; **19**: S95–S101.
31. White R, Granger DN. The peritoneal microcirculation in peritoneal dialysis. In: Gokal R, Khanna R, Krediet RT, Nolph KD (eds). Kluwer Academic Publishers: Dordrecht, 2000, pp. 107–133.
32. Ripley EB, Gehr TW, Kish CW, Sica DA. Hormonal, blood pressure, and peritoneal transport response to short-term ACE inhibition. *Perit Dial Int* 1994; **14**: 378–383.
33. Kim M, Lofthouse J, Flessner MF. Blood flow limitations of solute transport across the visceral peritoneum. *J Am Soc Nephrol* 1997; **8**: 1946–1950.
34. Combet S, VanLandschoot M, Moulin P *et al.* Regulation of aquaporin-1 and nitric oxide synthase isoforms in a rat model of acute peritonitis. *J Am Soc Nephrol* 1999; **10**: 2185–2196.
35. Lai KN, Li FK, Lan HY *et al.* Expression of aquaporin-1 in human peritoneal mesothelial cells and its upregulation by glucose *in vitro*. *J Am Soc Nephrol* 2001; **12**: 1036–1045.
36. Umenishi F, Schrier RW. Hypertonicity-induced aquaporin-1 (AQP1) expression is mediated by the activation of MAPK pathways and hypertonicity-responsive element in the AQP1 gene. *J Biol Chem* 2003; **278**: 15765–15770.
37. Roudier N, Verbavatz JM, Maurel C *et al.* Evidence for the presence of aquaporin-3 in human red blood cells. *J Biol Chem* 1998; **273**: 8407–8412.
38. Delporte C, O'Connell BC, He X *et al.* Adenovirus-mediated expression of aquaporin-5 in epithelial cells. *J Biol Chem* 1996; **271**: 22070–22075.
39. Chantrain CF, DeClerck YA, Groshen S, McNamara G. Computerized quantification of tissue vascularization using high-resolution scanning of whole tumor sections. *J Histochem Cytochem* 2003; **51**: 151–158.